

FUZZY POWER CONTROL FOR DOUBLY FED INDUCTION GENERATOR BASED WIND FARM

¹MOHAMED HILAL, ¹YOUSSEF ERRAMI, ¹MOHAMED BENCHAGRA,
¹MOHAMED MAAROUI

¹Dept. of Electrical Engineering, Ecole Mohammadia des Ingénieurs EMI,
Univ. Mohamed V-Agdal, Rabat, MOROCCO
E-mail: ¹hilalisme@gmail.com

ABSTRACT

This paper expands a nonlinear fuzzy based control strategy applied to a variable speed Wind Energy Conversion System WECS founded on Doubly Fed Induction Generator DFIG. As power network assists a high wind energy emergence, the studied WECS represents a wind farm WF of 500MW connected to the Grid and dispatched in such a way that it can contribute to grid frequency control with delivering a stable output equaling the power setpoint and keep a reserve for eventual increasing. Basing on the rotor currents maneuvering, the active power control is achieved independently to reactive power being adjustable according to grid request. The system is modeled using PSCAD/EMTDC linked to MATLAB for the fuzzy logic controllers FLC implementation. FLC are based on Takagi-Sugeno Fuzzy Logic Controller TSFC. Despite the wind speed fluctuations, results show a stable output following carefully a gradual change in power reference. Moreover, a THD analysis confirms the best quality of grid injected power.

Keywords: *Doubly Fed Induction Generator (DFIG), Fuzzy Logic Controller (FLC), Field Oriented Control (FOC), Wind Energy Conversion System (WECS)*

1. NOMENCLATURE

ρ, λ	Air Density, Tip Speed Ratio TSR
R_t, v_w	Turbine Radius, wind speed
C_p, β	Power Coefficient, Pitch angle
β_{ref}	Reference pitch angle
j, f	Turbine Inertia, Viscous friction
Ω_t, Ω	Turbine Speed, Mechanical speed
v_{ds}, v_{qs}	Direct and Quadratic Stator Voltages
$v_{as}^*, v_{bs}^*, v_{cs}^*$	VSC reference voltages in abc Frame
v_{d1}^*, v_{q1}^*	Dq VSC output Reference Voltages
i_{ds}^*, i_{qs}^*	Dq Stator reference Currents
$i_{as}^*, i_{as}^*, i_{as}^*$	Three phase stator reference currents
i_{dr}^*, i_{qr}^*	Dq Stator reference Currents
ψ_{ds}, ψ_{qs}	Direct, Quadratic Stator Flux
ψ_{dr}, ψ_{qr}	Direct, Quadratic Rotor Flux
M	Magnetizing inductance
$\theta_s, \theta_r, \theta_{slip}$	Stator, Rotor, Slip angle
ω_s, ω_r	Stator, Rotor Pulsation
P_s, Q_s, P_r, Q_r	Stator and Rotor Power
P_1, Q_1	Active reactive Inverter Power
T_{ir}, T_{ig}	Rotor, Grid side converter pulses
e, r	Error, Error rate
T_s	Sampling time period
R, L	transformer resistor, inductor
Γ_E, Γ_m	Electric, Mechanic Torque

2. INTRODUCTION

As result of world conscience on the worst impact of fossil energy on the whole life aspects, renewable energy emerges into the grid by replacing several conventional power sources. Wind energy having a randomized form should be trained using recent power electronic technologies to ensure a similar quality power of conventional sources. Any failure of the grid connected wind farm WF can be harmful for the whole power network. Thus, WF should be able to guarantee a stable output power for different wind speeds and participate actively in the power system operation as conventional power plants. Hence, the Power System Operators PSO have recently reviewed the Grid Codes Requirements GCR for wind farms including several control tasks. The generation control capability of both active and reactive power ranks among them [1] [2] [3].

After setting the output power consign, the rotation velocity varies considerably depending on the turbine mechanical torque MT and the electrical torque ET developed by the generator. However, it must remain in the proportion that allows the rotation speed in a secure margin. This range is bordered by the machine speed upper and lower limit. The Pitch angle is actuated to reduce MT on the shaft once speed increases over the reference

value. The velocity slowing down results in wind insufficiency to ensure the MT required for producing the demanded power.

The WF power consign should generally be less than the WF available power P_{Avail} given for the machine optimal speed corresponding to maximal power point tracking MPPT strategy. This is done in order to keep a power reserve for a possible increase in the setpoint, not only to make it able to contribute in grid frequency control by producing as much power as specified in the reference, but also to avoid power swings and smoothing the output. The P_{Avail} overtaking, subsists generally during short time leading to the speed slowdown, it is tolerable once the rotor possesses large kinetic energy allowing rotation continuity.

Latest years have witnessed fast emerging popularity of fuzzy control systems in engineering applications. The several successful FLC implantations have engendered a burst of activities in the analysis and design of fuzzy control systems. The growing integration of large WF into grid increases its control complexity which focuses on the plant modeling using differential equations. Wind variation and short term period of forecasting makes challenging the use of conventional control approaches based on the plant model. They require deep system knowledge and manage principally the plant governing equations. In fuzzy control, inspired by human reasoning based on experience, the focus is set on getting intuitive knowledge of the appropriate manner ensuring the best plant control. Then, decisions are loaded into the controller rule base to become a formal methodology for the control. This simplified structure, ordered in natural language terms, leads to an easier implementation and covers a wide range of operating conditions. The FLC decisions are taken according to the rule base built in such a way that it represents the human expertise. The rules are deduced generally from an expert having spent long time learning how best to control the process or by studying the system dynamics. [4] [5].

Our earlier works [6][7][8], consisting of studying various DFIG WF aspects under faulted and normal grid conditions use conventional approaches. In this work a new WF model is built based on fuzzy approach of the Takagi-Sugeno model which is different from the Mamdani one in a linear consequent that provides a wide range of control gain variation promising options for industrial applications with many desirable features.

Throughout this paper, we subjected our new model to a gradual increase of active power consign independently to reactive power. The simulation is done under variable wind speed; composed of four components: main, gust, ramp and noise to test WF in a realistic environment. This evaluates the model robustness and our parameters accuracy. The DFIG is driven over the rated speed for providing the rotor with large kinetic energy which can be restored when active power consign exceeds available power for output smoothing reasons.

3. STUDY SYSTEM DEPICTION

The WF aggregated model is reduced in a single wind turbine model with equivalent parameters. In the diagram given in Fig.1, the individual generators are lumped into an equivalent machine represented at the collector bus. This modeling method has large use in system studies [9]. It is interested in the whole system behavior and its interaction with surrounding items. The WF is modeled by a single equivalent machine connected to a transformer unit thereby forming an aggregated WF model. The studied WF rated power is 500 MW, formed by 250 WT with a rated power of 2 MW clustered in 10 rows.

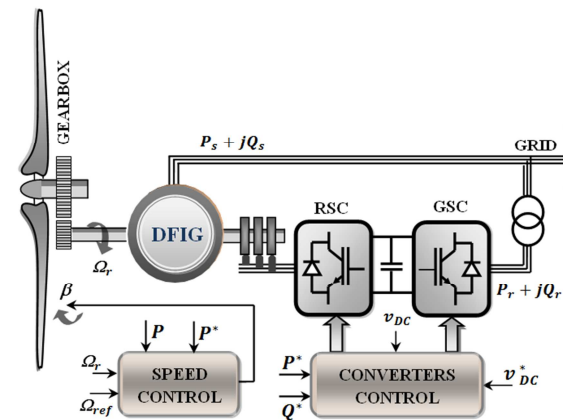


Figure 1. Modular diagram of Studied system.

The DFIG magnetizing is achieved via a direct link of the stator to the grid. In order to adjust rotation speed, the rotor is coupled to the grid through a Variable Frequency Converter VFC which sets the rotor currents frequencies according to desired velocity. Our interest in this work consists in generating the dispatched power while keeping DFIG velocity within the safe operating range. The FC is made of the rotor side converter RSC, the grid side converter GSC and the DC link which dissociates the fuzzy control of the two

PWM converters based on a vector control approach [10]-[12].

3.1. Aerodynamic model

Wind power crossing an area is given in (1). The WT aerodynamic blades transform a small part of wind power to mechanical power related to the mechanical torque in (2). The power coefficient in (3) specifies the extracted power proportion from wind. It depends essentially on the blades geometry and pitch angle. The three blades WT is the most used in the wind energy market thanks to its power coefficient reaching 50% [13].

$$P_{wind} = \frac{1}{2} \cdot \rho \cdot A \cdot v_{wind}^3 \quad (1)$$

$$\Gamma_m = \frac{\rho \cdot \pi \cdot R_t^2 \cdot v_w^3 \cdot C_p(\lambda, \beta)}{2 \cdot \Omega_t} \quad (2)$$

$$C_p(\lambda, \beta) = 0.52 \left(\frac{116}{\lambda_i} - 0.4\beta - 5 \right) e^{-\frac{21}{\lambda_i}} \quad (3)$$

$$\lambda_i^{-1} = \frac{1}{\lambda + 0.08\beta} - \frac{0.035}{\beta^3 + 1} \quad \lambda = \frac{R_t \cdot \Omega_t}{v_{wind}} \quad (4)$$

3.2. Mechanic Equation

The equation governing DFIG rotation (5) depends on the gap between electric torque issued from the generated power and the mechanic torque resulted in the extracted power from wind. This gap represents the rotor acceleration. The machine velocity results in mechanic torque that has a tendency to accelerate rotation whereas the electric one tends to slow it down. Sudden speed changes are due to electric torque spikes which should be smoothened in the control strategy.

$$J \cdot \frac{d\Omega}{dt} = \Gamma_m - \Gamma_E - f \cdot \Omega \quad (5)$$

3.3. Study WECS modeling

According to Field Oriented Control FOC aligning the flux field to the park frame direct axis and neglecting the per phase stator resistance which is the case for middle and high power generator the flux equations are given in (6)-(9).

$$\varphi_{dr} = L_r \cdot i_{dr} + M \cdot i_{ds} \quad (6)$$

$$\varphi_{qr} = L_r \cdot i_{qr} + M \cdot i_{qs} \quad (7)$$

$$v_{qs} = -\omega_s \cdot \varphi_{ds} \quad (8)$$

$$\varphi_{ds} = 0 \quad (9)$$

Mechanic torque resulting of the mechanical power on the shaft is given in (10). Electric torque driven with quadratic component of rotor current is specified in (11).

$$\Gamma_m = \Gamma_E + J \cdot \frac{d\Omega}{dt} + f \cdot \Omega \quad (10)$$

$$\Gamma_E = -\frac{3}{2} \cdot \frac{P \cdot M}{L_s} (\psi_{ds} \cdot i_{qr}) \quad (11)$$

The Stator active power controlled by the rotor current quadratic component is computed using (12). The reactive power controlled by the rotor current direct component is given in (13).

$$P_s = -\frac{3}{2} \frac{M}{L_s} v_{qs} \cdot i_{qr} \quad (12)$$

$$Q_s = \frac{3}{2} \left(\frac{v_{qs}^2}{\omega_s \cdot L_s} - v_{qs} \frac{M}{L_s} \cdot i_{dr} \right) \quad (13)$$

Rotor voltages are expressed in dq reference frame in (14,15).

$$v_{dr} = R_r \cdot i_{dr} + \frac{d\varphi_{dr}}{dt} - \omega_r \cdot \varphi_{qr} \quad (14)$$

$$v_{qr} = R_r \cdot i_{qr} + \frac{d\varphi_{qr}}{dt} + \omega_r \cdot \varphi_{dr} \quad (15)$$

4. FUZZY LOGIC CONTROLLER DESIGN

Despite the TSFC simplified representation, its design is very difficult. Various studies have been made to improve systematic TSFC design. The researchers have focused on how to develop an efficient and simple TSFC designing method.

4.1. Fuzzy regulator Structure

The FLC includes four main interactive mechanisms: The fuzzification unit determining inputs membership values to the fuzzy sets of the discourse universe. The Fuzzy Inference System FIS evaluates at each time which control rules are appropriate using the base knowledge. The defuzzification unit computes the crisp output of the rules leading to the optimal plant control. The typical TSFC configuration is given in Fig.2

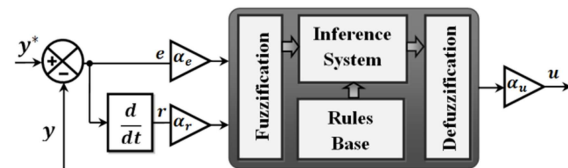


Figure 2. Fuzzy controller structure

$$e(nT_s) = y^*(nT_s) - y(nT_s) \quad (16)$$

$$r(nT_s) = e(nT_s) - e(nT_s - T_s) \quad (17)$$

Where n : Positive integer, T_s : Sampling time, y^* : Setpoint, $e(nT)$: Error, $r(nT)$: Error rate, $y(nT)$: system output.

In this work, the FLC design uses the hand-tuning method considering, in the first stage, the classical PI as a reference. The conventional PI is replaced by a Fuzzy PI with a discrete approximation depicted in (18). The same response

of the closed loop system verifies of the right implementation.

$$u_n = k_p \cdot \left(e_n + \frac{1}{T_i} \sum_{j=1}^n e_j \cdot T_s \right) \quad (18)$$

The defuzzification process computes output with assigning a representative value to the fuzzy variable. The output of the TS model is calculated by the weighted average given in (19)

$$u^* = \frac{\sum_{i=1}^m \mu(x_i) \cdot x_i}{\sum_{i=1}^m \mu(x_i)} \quad (19)$$

4.2. Membership functions

The highest excursion of the inputs is scaled to the input universe in order to avoid saturation. The signals sizing are obtained with adjusting the FLC gains. To increase sensitivity, the input universe is split into seven triangular sets crossing their adjoining at the medium membership value as depicted in Fig.3. This provides a sufficient sensitivity in the case study. The output sets are reduced to singleton to simplify the Center Of Gravity COG defuzzification algorithm. Every small area of the FLC transfer map can be easily adjusted with simply adapting the relating rules which allows a local fine-tuning of the response for each value of the inputs. This provides FLC with a soft configuration leading to a powerful flexibility.

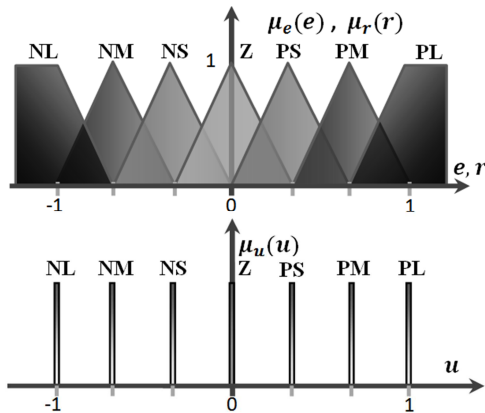


Figure 3. Input-Output membership function

4.3. Fuzzy regulator tuning

For FLC simple designing, it is split into decoupled proportional and integral fuzzy regulators. The hand-tuning first stage acts on the Fuzzy Proportional regulator gains. The fine-tuning is obtained in the second stage by adjusting the

integral gain to remove any final value offset. The relating diagram is depicted in Fig.4.

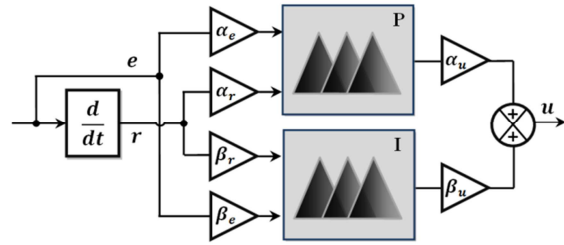


Figure 4. Proportional and Integral Fuzzy controller

The FLC response is illustrated in (20) where f_p and f_i are nonlinear functions. A linear approximation is done to find approximate values of the FLC gains to be used in the first step of the tuning method. This reduces considerably the tuning time.

$$u_n = f_p(\alpha_e \cdot e_n, \alpha_r \cdot r_n) \cdot \alpha_u + f_i(\beta_e \cdot e_n, \beta_r \cdot r_n) \cdot \beta_u \quad (20)$$

The tuning approach sets individually gains for each FPI regulator and considers the conventional PI response as a reference to compare the FPI response with. The generic TS rule has the following syntax:

$$R_k : \text{ If } e \text{ is } A_{k1} \text{ AND } r \text{ is } A_{k2} \\ \text{ THEN } y_k = f_k(x_1, x_2) ;$$

The proportional FLC governing rules used in this work are collected in TABLE.1. It assigns the output membership fuzzy set related to the inputs fuzzy sets

TABLE 1. KP-FUZZY CONTROL RULE BASE

e \ r	NL	NM	NS	Z	PS	PM	PL
NL	PL	PL	PM	PM	PS	PS	Z
NM	PL	PL	PM	PM	PS	Z	Z
NS	PM	PM	PM	PS	Z	NS	NM
Z	PM	PS	PS	Z	NS	NM	NM
PS	PS	PS	Z	NS	NS	NM	NM
PM	Z	Z	NS	NM	NM	NM	NL
PL	Z	NS	NS	NM	NM	NL	NL

The proportional FLC transfer surface is depicted in Fig.5.

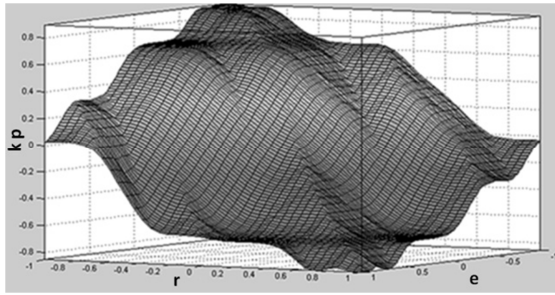


Figure 5. Control Surface of Proportional FLC

TABLE.2 assembles the integral FLC rules.

Table 2. Ki-Fuzzy Control Rule Base

r \ e	NL	NM	NS	Z	PS	PM	PL
NL	NL	NL	NL	NM	NM	Z	Z
NM	NL	NL	NM	NM	NS	Z	Z
NS	NM	NM	NS	NS	Z	PS	PS
Z	NM	NS	NS	Z	PS	PS	PM
PS	NS	NS	Z	PS	PS	PM	PM
PM	Z	Z	PS	PM	PM	PL	PL
PL	Z	Z	PS	PM	PL	PL	PL

The mapping of the integral FLC transfer map is illustrated in Fig.6.

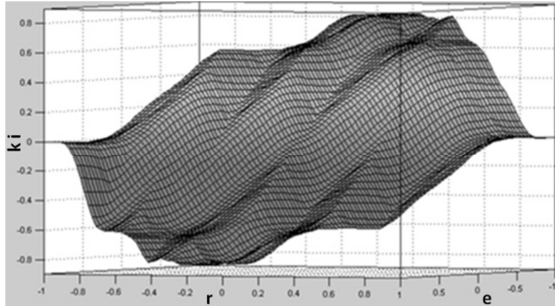


Figure 6. Control Surface of Integral FLC

5. CONTROL STRATEGY

The VFC dimensioning depends mainly on the power part flowing through. The rotor power represents 30% against the stator's share reaching 70%. This reduces converter sizing and gives doubly fed induction generator DFIG a particular strength in wind power markets. Despite brushes maintaining, it stands as the mainstream design for large wind turbines [14]. The VFC is made of RSC, GSC and the DC link which dissociates the control of the two PWM converters. GSC regulates DC voltage with unity power factor through the inverter whereas RSC generates rotor reference currents to be injected in the rotor windings.

5.1. Rotor-Side Converter Control

The rotor reference currents are computed in terms of the gap between the sensed and the ordered powers as depicted in Fig.7. The resulted reference rotor currents are translated to abc frame depending on slip angle. RSC firing pulses are generated using Current Reference Pulse Width Modulation CRPWM. As pitch mechanism acts slowly, sudden changes in dispatched power are avoided to prevent electric torque peaks [15].

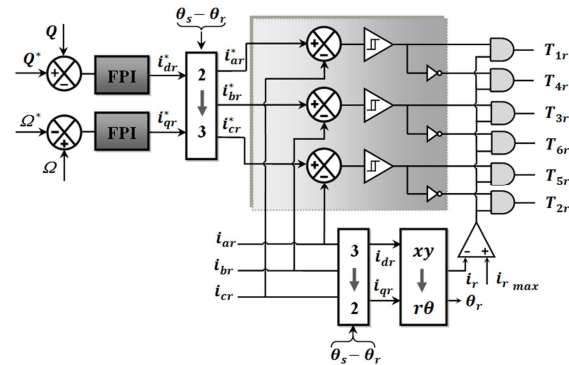


Figure 7. Rotor side control.

Rotor currents are limited to protect IGBTs and rotor windings from excessive currents. When this limit is reached RSC pulses are disabled.

5.2. Grid-side converter

Aligning the grid voltage to the direct axis of park frame to fulfill FOC conditions. The simplified equation linking grid voltages to the GSC output voltage and currents is given in (21) where R and L are respectively the per phase transformer resistor and inductor.

$$\frac{d}{dt} \begin{bmatrix} i_{d1} \\ i_{q1} \end{bmatrix} = \begin{bmatrix} -R & \omega_s \\ L & -R \\ \omega_s & -R \\ L & L \end{bmatrix} \cdot \begin{bmatrix} i_{1d} \\ i_{1q} \end{bmatrix} + \begin{bmatrix} v_{dg} - v_{d1}^* \\ 0 - v_{q1}^* \end{bmatrix} \quad (21)$$

The active and reactive power transiting through the inverter are simplified to expressions in (22,23)

$$P_1 = \frac{3}{2} v_G \cdot i_{d1} \quad (22)$$

$$Q_1 = -\frac{3}{2} v_G \cdot i_{q1} \quad (23)$$

Hence, a decoupled control of active and reactive power flowing through the inverter is achieved. The active power crossing the inverter is regulated to permit a constant power of the capacitor leading to a stable DC bus voltage. The regulation is done considering P_r as a perturbation.

$$\frac{1}{2} C \frac{dv_{DC}^2}{dt} = P_1 - P_r \quad (24)$$

The remaining concern is to decouple control between direct and quadratic inverter currents because in (21), a change in each component causes a transient change in both power components. A decoupled control is insured using (25).

$$\frac{d}{dt} \begin{bmatrix} i_{1d} \\ i_{1q} \end{bmatrix} = \begin{bmatrix} -R/L & 0 \\ 0 & -R/L \end{bmatrix} \cdot \begin{bmatrix} x_1 \\ x_2 \end{bmatrix} \quad (25)$$

$$x_1 = \frac{v_{dg} - v_{1d}^*}{L} + \omega \cdot i_{1q} \quad x_2 = \frac{-v_{1q}^*}{L} - \omega \cdot i_{1d}$$

$$v_{1d}^* = -L \cdot x_1 + v_{dg} + \omega \cdot L \cdot i_{1q}$$

$$v_{1q}^* = -L \cdot x_2 - \omega \cdot L \cdot i_{1d}$$

As depicted in Fig.8, The gap between the sensed value and the reference of DC Bus voltage drives direct current component. The quadratic one is kept null for unity power factor through the inverter. Grid reference voltages are deduced after resulting currents regulation. The IGBTs firing pulses of GSC are generated using Sinus Pulse Width Modulation SPWM.

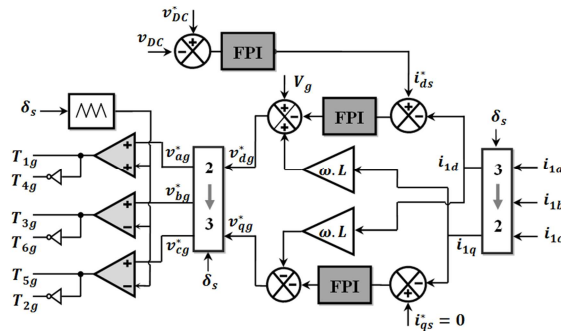


Figure 8. Grid side control

5.3. Pitch Control

DFIGWT power generation can be produced with variable speed ranging from sub-synchronous to super-synchronous, giving a significant excursion which can be used to store wind power in rotor kinetic energy and restore it for smoothing electric power output. DFIG velocity margin is limited between two values depending on the machine maximum and minimum slip. In this work, the reference rotor speed is set 10% above the generator rated speed in order to store large kinetic energy in the rotor. It is done in super-synchronous margin lowering detriment. Fig.9 shows the generated power in the operating speed range with the reference speed in the asymmetric center.

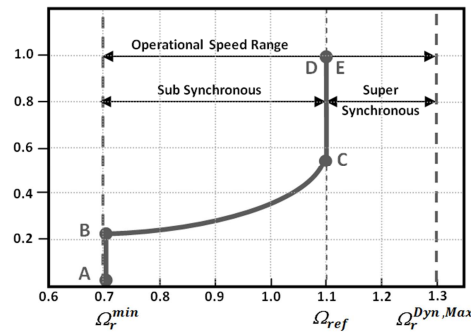


Figure 9. Electric Power vs Operating Speed Range.

This irregularity has less effect since pitch system reduce the torque on the shaft by operating in normal mode at speed (10°/s) or during urgent situations in which blades are pitched at speed (20°/s). In most WT a braking system is used to assist the pitch control during emergency [17]. Fig.10 depicts The adopted pitch system model

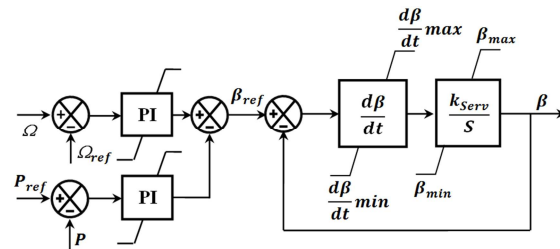


Figure 10. Pitch system regulator

Since the power gap is minimal, thanks to the closely tracking, it is rather the rotor speed variations which are in the origin of pitch angle actuating when overtaking the reference speed.

5.4. Frequency Control Ability

As illustrated in Fig.11, for dynamic participation in grid control, WF should fulfill the TSO requests as increasing active or reactive reference. Hence, WF should produce a share of its installed power so as to keep a reserve for ultimate references increase.

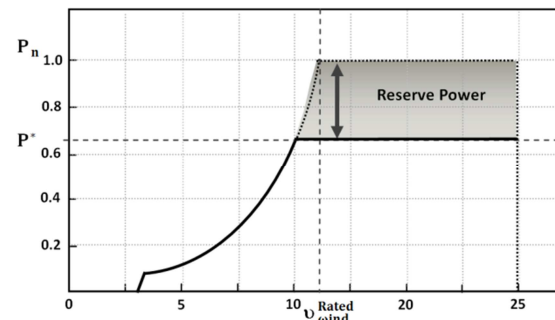


Figure 11. Electric Power vs wind speed

6. SIMULATION RESULTS

FLC algorithms are implemented in an m-file of MATLAB. The WF model is achieved using PSCAD/EMTDC. A link between the software is made using a FORTRAN unit for running the fuzzy algorithm.

Simulation starts at speed mode which carries generator speed to 10% over the rated value. And then switched over to torque control at 0.5s, after the initial transients of the machine die out. The wind farm model is subjected to variable wind speed to be experienced in realistic conditions. The wind components are: main (9m/s), gusts (0.5m/s), ramp (0.5m/s) and noise. The wind profile is depicted in Fig.12.a.

A gradual active power rising consist 10%, 22%, 34%, 46% and 58% of the WF rated power is dispatched, the power increasing steps are assumed to highlight WF dynamic response for a variable power consign. Fig.12.b displays both active power curves of PQ and MPPT control in order to compare extracted power with the available power under the same wind speed. We clearly see the fuzzy control benefits in the generated power being smoothed although available power lowering below the dispatched reference which justifies the fact of driving DFIG at over speed.

The brief change in reference power causes electric torque peaks causing stress and damaging the shaft. Those peaks are depicted at 1s and 2s of simulation time in Fig.12.c. It corresponds to sudden change in dispatched power at the related time steps in Fig.12b. To avoid sudden changes and minimize the inflicted electrical and mechanical stress, the power consign should vary slowly. It is done simply by a rate limiter. For the next steps at 3s and 4s of the simulation time, peaks are avoided.

Pitch angle evolution is depicted in Fig.12.d. It is actuated when requested power is small in power to reduce mechanic torque and adapt it to the electric one. The extracted power from wind is not maximal, as shown in Fig.12.e displaying, for comparison, both power coefficient curves of PQ demand and MPPT request. The turbine extracts only the sufficient fraction for producing demanded power. Blades are pitched in normal mode with reserving emergency ones for high gusts and turbulences. The highest pitching rate during the whole simulation time is (8°/s).

Fig.12.f depicts both curves of rotor speed evolution relating to PQ and MPPT requests. In

both curves the speed is ranged in the secure margin although wind variations by using only pitch system operating in normal mode with a variation rate less than (10°/s).

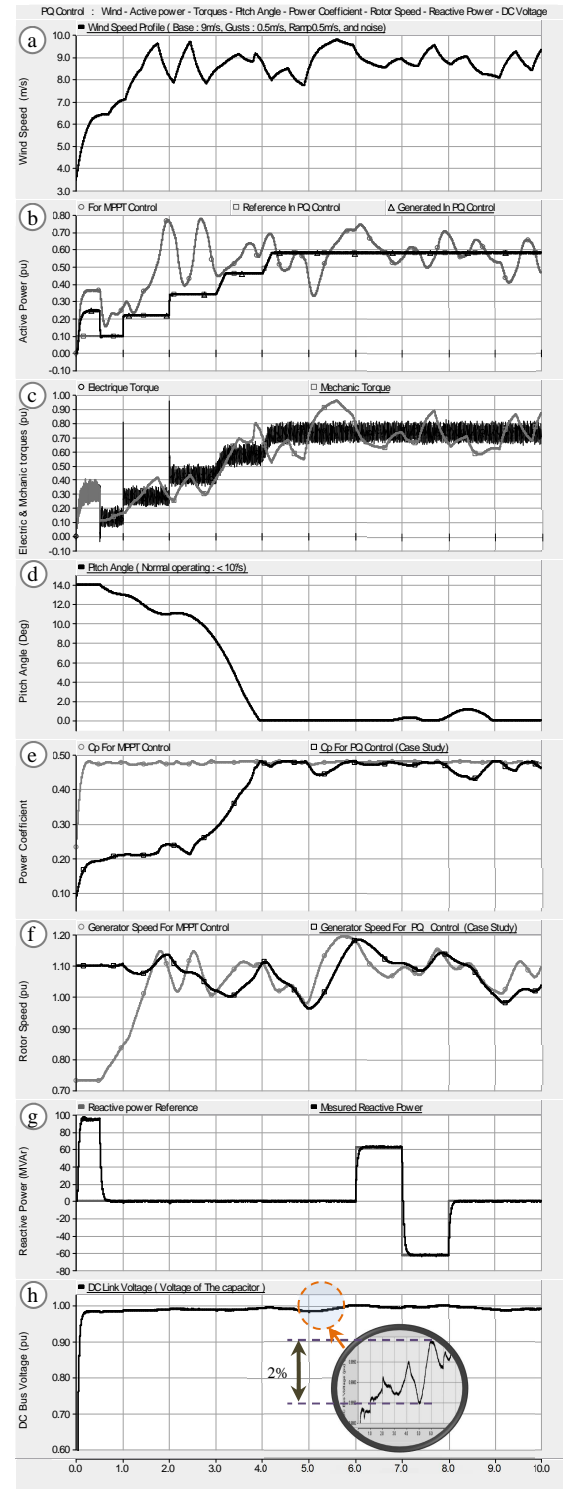
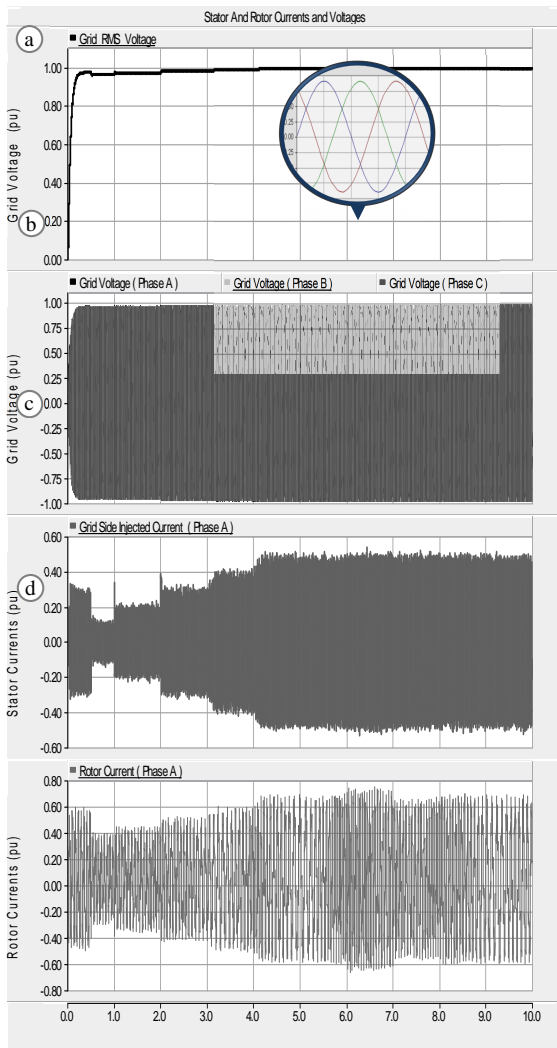


Figure 12. Simulation resulting curves.

The WF active and reactive powers have followed closely their requests in perfect independency. First, a WF unity power factor is dispatched. We also set reactive power setpoint to 64MVAR to demonstrate that WF can provide reactive power to grid if needed. Again to -64 MVAR to illustrate that it can also absorb reactive power as represented in Fig.12.g. This confirms the fuzzy decoupled control of active and reactive power.

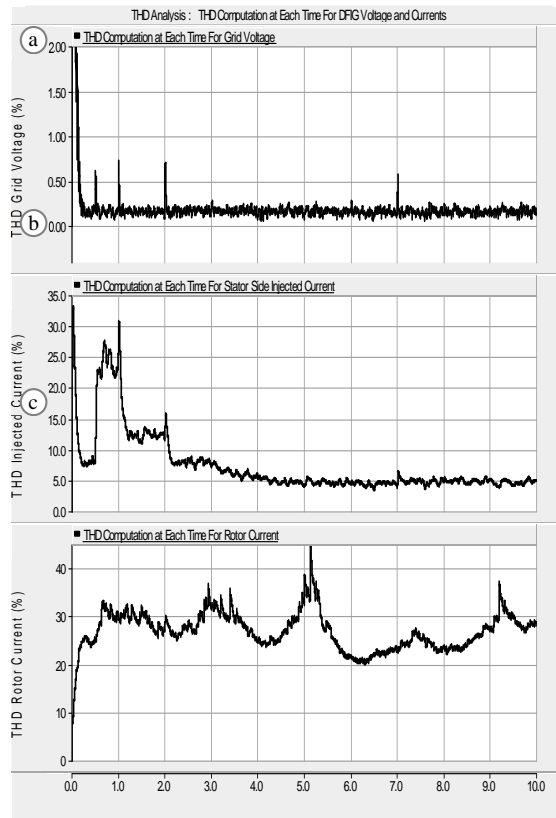
DC voltage given in Fig12.h is stable around the rated value with a maximal excursion less than 2% which attests the GSC fuzzy control effectiveness.

Grid voltage is illustrated in Fig.13.b with its RMS value depicted in Fig.13.b. The Injected current depiction is given in Fig.13.c illustrating the injection in the stator side and in Fig.13.d relating to the rotor currents.



The WECS based on static converters presents generally distorted voltages and currents wave forms. In this work, a THD analysis is adopted to highlight the impact of the WECS based on fuzzy regulators going on the power quality grid injection.

A small power part follows through the FC in charge of the current distortion. The GSC currents are filtered by the transformer before being injected into grid. Moreover, FLC ensure, by a soft control, a smooth current injection avoiding the surpassing well-known of the PI regulators. The curves attest the best wave forms of the grid voltage and current. As DFIG is current controlled a minor distortion is noticeable on the rotor current wave form due to converters switches. Fig.14.a shows the THD of grid voltage limited to 0.5% attesting a minor influence. Fig.14.b depicts the THD of grid injected currents at the stator side with a maximum distortion of 6%. As shown in Fig.14.c, the currents flowing through the frequency inverter reach a THD level of 25%. However, those currents represent a small fraction of the total injected currents since the major part flows through the stator side. Moreover, they are smoothed by the transformer inductors.



7. CONCLUSION

WECS assisted significant improvements in recent years concerning their control and design. Wind farms installed power growth amplifies power network complexity challenging conventional approaches based on the plant modeling. Minimal knowledge and simplified structure are sufficient for FLC to control complex systems. However, grid faults with grid codes requirements provide a second challenge which requires more innovative control.

The FLC based control strategy has proved the theoretical analysis and provides an independent, soft and flexible active and reactive power control. Furthermore, output power is smoothed despite wind fluctuations which is commonly needed in grid connected WF. This approach qualifies the WF to contribute in grid frequency control. The rotor can store kinetic energy when it is driven over its rated speed. This energy can be restored during small winds causing speed lowering but the trip remains in the operating range.

The TS fuzzy controller, although missing a systematic design method, are characterized by simplicity, a low memory occupancy, fault tolerance, learning ability and flexibility confirmed by the ability of adapting the response of a transfer map area with simply adapting the few relating FIS rules which promotes TSFC in complex plants control. Our future work will be on applying fuzzy approach on DFIG fault ride through capability.

REFERENCES:

- [1] J. Morren and S. W. H. Hann, "Ridethrough of wind turbines with doubly-fed induction generator during a voltage dip," *IEEE Trans. Energy Conv.* Vol. 20, no 2 June 2005.
- [2] Jauch C, Matevosyan J, Ackermann T, Bolik S. International comparison of requirements for connection of wind turbines to power systems. *Wind Energy* 2005;8:295–306.
- [3] Mikel Alberdi, Modesto Amundarain, Aitor J.Garrido, Izaskun Garrido, Francisco Javier Maseda, "Fault-Ride Through Capability of Oscillating-Water-Column-Based Wave Power Generation Plants Equipped With Doubly Fed Induction Generator and Airflow Control", *IEEE Trans.on Industrial Electronics*, Vol.58,No.5, May2011, pp. 1501-1517.
- [4] Tomonobu Senjyu , Toshiaki Kaneko , Akie Uehara , Atsushi Yona , Hideomi Sekine , Chul-Hwan Kim , "Output power control for large wind power penetration in small power system", *Elsevier Renewable Energy* 34 (2009) 2334–2343
- [5] Péter Baranyi, Yeung Yam, Annamária R. Várkonyi-Kóczy, Ron J. Patton , "SVD-Based Reduction to MISO TS Models", *IEEE Trans. Industrial Electronics*, VOL. 50, NO. 1, FEBRUARY 2003
- [6] Mohamed HILAL, Mohamed MAAROUFI, "Power Network Control and Management", *The 1th International Conference on Multimedia Computing and Systems, IEEE-ICMCS'09~*, April 2-4, 2009, Ouarzazate, Morocco.
- [7] M. Hilal, M. Maaroufi, M. Ouassaid, "Doubly fed induction generator wind turbine control for a maximum power extraction", *The 2th International Conference on Multimedia Computing and Systems, IEEE-ICMCS'11~*, April 7-9, 2011, Ouarzazate, Morocco.
- [8] M. Hilal, M. Benchagra, Y. Errami, M. Maaroufi, M. Ouassaid , "Maximum Power Tracking of Wind Turbine based on Doubly Fed Induction Generator", *International Review on Modelling and Simulations*, Vol. 4, n. 5, November 2011, pp. 1007-1014
- [9] Anca D. Hansen, Florin Iov, Poul Sørensen, Nicolaos Cutululis, Clemens Jauch, Frede Blaabjerg Risø-R-1400 "Dynamic wind turbine models in power system simulation tool DIgSILENT", *Risø National Laboratory, Technical Univ. Denmark Roskilde*, August 2007.
- [10] Vladislav Akhmatov, "Analysis of dynamic behavior of electric power systems with large amount of wind power", *Ph.D thesis Technical University of Denmark*, April 2003
- [11] R. Pena, J.C. Clare and G.M. Asher, "Doubly fed induction generator using back to back PWM converters and its application to variable speed wind energy generation," *IEE Proc. Electrical Power Applications*, Vol. 143., No.3., May 1996.
- [12] J. G. Sloopweg, S. W. H. de Haan, H. Polinder, and W. L. Kling, "Modeling wind turbine in power system dynamics simulations," in *Proc. IEEE Power Engineering Society Summer Meeting, Vancouver, BC, Canada*, Jul. 2001, pp. 15U" 19.



- [13] T. Sun, Z. Chen, and F. Blaabjerg, "Transient analysis of grid-connected wind turbines with DFIG after an external short-circuit fault," *Nordic Wind Power Conf., Chalmers Univ. Technol.*, Gothenburg, Sweden, Mar. 2004.
- [14] J. B. Ekanayake, L. Holdsworth, X. G. Wu, and N. Jenkins, "Dynamic modeling of doubly fed induction generator wind turbines," *IEEE Trans. Power Electron.*, vol. 18, no. 2, pp. 803–809, May 2003.
- [15] Sørensen P., Bak-Jensen B., Kristiansen J., Hansen A.D., Janosi L., & Bech J. Power plant characteristics of wind farms. Wind Power for the 21st Century. *the International Conference, Kassel*, 2000, 6pp.
- [16] H. Faïda, J. Saadi, Modelling, Control Strategy of DFIG in a Wind Energy System and Feasibility Study of a Wind Farm in Morocco, *International Review on Modelling and Simulations*, Vol. 3, n. 6, December 2010, pp. 1250-1262
- [17] Brice Beltran, Mohamed Benbouzid, Tarek Ahmed-Ali, Hervé Mangel, DFIG-Based Wind Turbine Robust Control Using High-Order Sliding Modes and a High Gain Observer, *International Review on Modelling and Simulations*, Vol. 4, n. 3, June 2011, pp. 1148-1155